Molecular Crystals and Liquid Crystals

ISSN: 1542-1406 (Print) 1563-5287 (Online) Journal homepage: http://www.tandfonline.com/loi/gmcl20

Synthesis, crystal structure, thermal analysis and biological activities of sodium 5-carboxy-2,3-dihydroxybenzenesulfonate

J. Wei, K. Liu, F. Lin, Y. Zhou, J. Zou & C. Lin

To cite this article: J. Wei, K. Liu, F. Lin, Y. Zhou, J. Zou & C. Lin (2016) Synthesis, crystal structure, thermal analysis and biological activities of sodium 5-carboxy-2,3-dihydroxybenzenesulfonate, Molecular Crystals and Liquid Crystals, 629:1, 165-177, DOI: 10.1080/15421406.2015.1108149

To link to this article: http://dx.doi.org/10.1080/15421406.2015.1108149

Published online: 16 Jun 2016.

MOLECULAR CRYSTALS AND LIQUID CRYSTALS
2016, VOL. 629, 165–177
http://dx.doi.org/10.1080/15421406.2015.1108149

Taylor & Francis
Taylor & Francis Group

Synthesis, crystal structure, thermal analysis and biological activities of sodium 5-carboxy-2,3-dihydroxybenzenesulfonate

J. Wei[a,b], K. Liu[a,b], F. Lin[c], Y. Zhou[a,b], J. Zou[a,b], and C. Lin[a,b]

[a]College of Chemistry and Chemical Engineering, Guangxi University, Nanning, China; [b]Guangxi Colleges and Universities Key Laboratory of Applied Chemistry Technology and Resource Development, Nanning, China; [c]Department of Hematology, the First Affiliated Hospital of Guangxi Medical University, Nanning, China

ABSTRACT

Through the sulfonation of protocatechuic acid, sodium 5-carboxy-2,3-dihydroxybenzenesulfonate (**SPA**) was synthesized. The structure of the sulfonated derivative was confirmed by FT-IR, MS, ^{1}H NMR, ^{13}C NMR, single crystal X-ray diffraction, and thermogravimetric analysis. The antioxidative activities of the derivative **SPA** were evaluated using 1,1-diphenyl-2-picrylhydrazyl (DPPH) scavenging method and reducing power determination, showing that **SPA** had strong antioxidative effects. Meanwhile DPPH scavenging progress by **SPA** was analyzed from dynamics experiments. Isothermal titration calorimetry (ITC) and circular dichroism (CD) were applied to investigate the interaction between the derivative **SPA** and human serum albumin (HSA).

KEYWORDS

Antioxidative activity; circular dichroism; crystal structure; isothermal titration calorimetry; protocatechuic acid; thermogravimetric analysis

Introduction

Phenolic acids have been found to be the secondary plant metabolites, which are universally distributed in nature plants and plant-derived foods [1]. The name "phenolic acids," means phenols that have one carboxylic acid functionality [2]. Phenolic acids are regarded as natural bioactive compounds, such as pro-coagulant, antifungal, anti-inflammatory, antioxidant, anticancer, antidiabetic, and antibacterial activities [3].

Protocatechuic acids (**PA**) contain hydroxybenzoic structures in naturally occurring phenolic acids and are present in nearly all plants [4]. Protocatechuic acid is one of the active constituents in Chinese medicines. There has been growing evidence that protocatechuic acid possesses strong antioxidant activity [5]. Protocatechuic acids are considered to be utility raw materials to create new value-added products. Antioxidants can inhibit oxidation processes and protect the body from damaging oxidation reactions, thus show beneficial health-promoting effects. In the past decades, the preparation of antioxidant compounds has become a research hotspot in pathological conditions, dietary and pharmacological uses [6].

As the abundant protein in blood plasma, serum albumin has many physiological functions and plays a key role in maintaining osmotic pressure and reversibly binding to endogenous and exogenous substances [7]. Ligands which bound to serum albumin with a high affinity may influence the bioavailability and efficacy of the drug in vivo.

CONTACT K. Liu kunliuuw@gxu.edu.cn C. Lin cuiwulin@163.com
Color versions of one or more of the figures in the article can be found online at www.tandfonline.com/gmcl.

In our previous research, it also can be found that a series of phenolic acids and their derivatives can bind to bovine serum albumin with high possibility so that they can be carried out by serum albumin to the targets in therapy [8]. Nowdays, as an established and invaluable method isothermal titration calorimetry (ITC) is applied to discover protein interaction with other proteins, small molecules, nucleic acids, carbohydrates, etc. [9]. Thermodynamic parameters determined quickly and accurately characterized from ITC experiments will provide the knowledge of manufacturing conditions. The information is essential in drug design and subsequent performance of pharmaceutical formulations [10].

In this study, a sulfonated derivative of protocatechuic acid, sodium 5-carboxy-2,3-dihydroxybenzenesulfonate (**SPA**), was synthetized. The crystal structure of **SPA** was confirmed by spectral methods (MS, IR, and NMR), X-ray crystallography and thermogravimetric analysis. The antioxidant activities of **SPA** have been investigated by scavenging 1,1-diphenyl-2-picrylhydrazyl (DPPH) assay and reducing power determination. Our data demonstrate that **SPA** elicited pronounced antioxidant effects. The investigation of the binding between **SPA** and human serum albumin (HSA) was proposed by isothermal titration calorimetry measurements. The binding constant K_b suggests that **SPA** binds strongly with HSA. In circular dichroism (CD) study there are no perceptible conformational changes in the secondary structure of the protein HSA in the presence of different molar concentration ratios of **SPA**.

Experimental

Materials and instruments

DPPH (2, 2-diphenyl-1-picrylhydrazyl) was biological reagent, purchased from Aladdin-reagent (Shanghai, China). Phosphate buffer (powder, Fuzhou Maixin Biotechnology Limited Company, China) was used to prepare a buffer solution (0.01 M, pH 7.4). Human serum albumin (HSA, 98%) was purchased from Sigma−Aldrich of biological grade. All other reagents were commercial materials of analytical purity without further purification. Doubly distilled water was used throughout.

Infrared spectra were recorded on a Tensor27 FTIR spectrometer (Bruker, Germany) using KBr pellets. Mass spectra were collected using a LC-MS 2010A (Shimadzu, Japan). ^{1}H and ^{13}C NMR spectra were carried out in D_2O on a Bruker Ascend^{TM} 600 at 600 MHz for ^{1}H and 150 MHz for ^{13}C, respectively. Uncorrected melting points were measured on an X-4 microscopic melting point apparatus (Beijing Technology Instruments, China). The pHs-3C digital pH meter with a combined glass calomel electrode was made in Shanghai Leici Device Works, China. The UV absorption spectra were recorded on a 7600 double beam UV/visible spectrophotometer (Shanghai Jinghua Instruments, China) using a 1.0 cm quartz cell. The X-ray crystallographic study was carried out using Bruker SMART CCD diffractometer with graphite monochromated Mo-K_α radiation ($\lambda = 0.71073$ Å) at $T = 296(2)$ K. Thermogravimetry analyses were performed on NETZSCH STA 449F3 ultra high temperature thermal analyzer (German). Isothermal titration calorimetry experiments were performed using an isothermal titration calorimeter called MicroCal ITC 200 from GE, USA. Circular dichroism spectrum was measured on MOS−450 circular dichroism spectrometer (BioLogic Science Instruments, France).

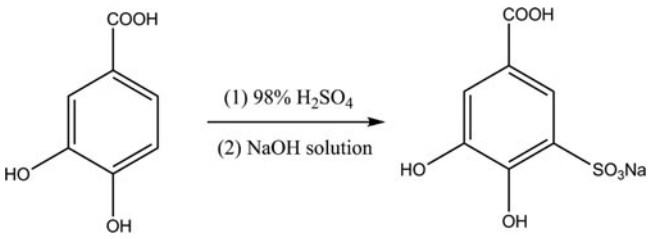

Figure 1. The synthesis route of sodium 5-carboxy-2,3-dihydroxybenzenesulfonate (**SPA**).

Synthesis

Synthetic method referred to the literature [11] and modified in this experiment. Into 60 mL concentrated sulfuric acid (98%, 1.2 mol) protocatechuic acid (30.8 g, 0.2 mol) was added and stirred for 8 h at 120°C. The thick, gray, treatable mass was poured into water in ice bath and it dissolved completely. Appropriate sodium hydroxide solution was mixed into the yellow product solution dropwise and then the white crude product was precipitated. Crystal **SPA** was obtained after crystallization in water at room temperature. The synthesis route was shown in Fig. 1.

Sodium 5-carboxy-2,3-dihydroxybenzenesulfonate (**SPA**) was obtained as colorless block crystal. Yield: 55.8%. melting point: >300°C, ^{1}H NMR (600 MHz, D_2O): δ 7.87 (d, J = 1.80 Hz, 1H); 7.48 (d, J = 1.80 Hz, 1H) ppm. ^{13}C NMR (150 MHz, D_2O): δ = 169.11, 146.84, 144.67, 127.84, 121.16, 120.86 and 119.12 ppm. FT-IR (KBr) ν: 3413, 3060 (m, Ar–OH), 1680 (s, >C=O), 1598, 1514 (Ar-H), 1385, 1187 (s, -SO_3-) cm^{-1}. ESI– MS (m/z): 233.2 (calcd 256.17 for $C_7H_5NaO_7S$, M-23).

Thermal analysis

NETZSCH STA 449F3 thermal analyzer was used to record TG and DTG curves at a heating rate of 10°C/min and heating programme 25–800°C. High purity nitrogen gas (99.999%) was used as static air atmosphere, flowing at 20 mL/min.

Antioxidant activities. Scavenging effect on DPPH radical

DPPH radical scavenging effect introduced by Blois [12] has been constantly used to measure the antioxidant potential. When dissolved in ethanol, DPPH can show a strong absorption band at 517 nm owing to the deep violet color of its solutions. A series of different volumes of **PA** (1 mM, in ethanol) and **SPA** solutions (1 mM, in water), varied from 0 to 1.0 mL, were added into 10 mL colorimetric tubes containing 1.0 mL DPPH solution (1 mM, in ethanol) and then diluted to 10 mL with ethanol. The final concentrations of DPPH were all 0.1 mM. After 30 min away from the light, the absorbance A_i was measured at 517 nm. In the same way, a series of different volumes of sample solutions were diluted to 10 mL with ethanol and the absorbance A_j was collected. Ascorbic acid was used as a positive control. All the tests were performed in triplicate. DPPH radical scavenging activities (RSA, %) of the sample solutions were calculated as the following equation:

$$RSA(\%) = 1 - \frac{A_i - A_j}{A_0} \times 100 \quad (1)$$

where A_i is the absorbance after 30 min scavenging reaction and A_j is the absorbance of the sample solutions with final concentrations ranging from 0.05 to 0.1 mM without DPPH. The blank control A_0 is the absorbance of DPPH solution without samples.

Radical scavenging activity is frequently expressed by calculating the values of inhibitory concentration 50 (IC_{50}), at which the initial DPPH radical concentration is decreased by 50%. The values of IC_{50} were obtained from the inhibition rates of curve fitting calculation.

The kinetics assay of scavenging effect on DPPH radical by **SPA** was also carried out, which was as same as that used in the above colorimetric method. Seven different volumes (100 μL, 200 μL, 300 μL, 400 μL, 500 μL, 800 μL, and 1000 μL) of **SPA** solution (1 mM, in water) were mixed with 1.0 mL DPPH solution (1 mM, in ethanol) respectively and then diluted to 10 mL with ethanol. The absorption at 517 nm was determined immediately after shaking and was read once per 5 min for 40 min. DPPH radical scavenging activities (RSA,%) at 40 min was also determined according to the equation (1). Then the kinetics curve was drawn according to the radical scavenging activities-time.

Reducing power determination

As early as 1986 Oyaizu [13] had performed the determination of the reducing power. In this assay, the reducing power of the samples was measured, following the method of Hayat [14]. A series of different concentrations of **PA** and **SPA** solutions (0–1.0 mM) 1.0 mL were mixed, respectively, with 2.5 mL phosphate buffer (0.2 M, pH 6.6) and 2.5 mL potassium ferricyanide (1% w/v). The mixtures were incubated at 50°C for 20 min, followed by the addition of 2.5 mL trichloroacetic acid (10% w/v). After centrifugation for 10 min, the supernatants (2.5 mL) were transferred into tubes with 2.5 mL distilled water and 0.5 mL ferric chloride (0.1% w/v). The absorbance of final mixture was collected at 700 nm. Ascorbic acid was used as a positive control. The blank control contained all the reagents except the samples. All the tests were performed in triplicate.

Isothermal titration calorimetry measurements [15]

HSA was dialyzed thrice against 0.01 M phosphate buffer (pH 7.4), and **SPA** was dissolved in the third dialysate. The pH value of the **SPA** solution was adjusted to close to that of the protein solution (with difference no more than 0.05). All solutions were thoroughly degassed before use. A typical titration involved 19 injections of the **SPA** called titrant (0.4 μL aliquot per injection from a 1000 μM stock solution) at 150 second intervals into the sample cell (volume 200 μL) containing HSA (50 μM) while stirring at 1000 r/min. The heat of the **SPA** solution dilution in the buffer alone was subtracted from the titration data in blank experiment. The experimental temperature was kept at 25°C. The data were analyzed with one binding site model using the Origin 7 software provided by MicroCal.

Circular dichroism spectroscopy [16]

The concentration of HSA was 1.0×10^{-5} mol/L in phosphate buffer. The **SPA** stock solution (1.0×10^{-4} mol/L) was prepared in the same buffer. Circular dichroism (CD) experiments of HSA were performed for the $C_{\mathbf{SPA}}$:C_{HSA} molar ratios as 0:1, 0.3:1, 0.7:1, 1:1, 2:1, and 3:1. The scanning was in the range of 200–260 nm. The phosphate buffer solution was selected as blank and was automatically subtracted during scanning. The temperature of the measurements was controlled at 25 $\pm$ 0.1°C. The average of three scans was recorded.

Results and discussion

Chemistry

Synthesis of the sulfonated derivative was performed according to the reaction exhibited in Fig. 1. The target compound was confirmed by FT-IR, MS, ^{1}H NMR, ^{13}C NMR, UV, single crystal X-ray diffraction, and thermogravimetric analysis.

The IR spectrum of the product exhibited absorption peaks at 1598 and 1514 cm^{-1}, assigned to C=C stretch for aromatic ring. The stretching frequency at 1680 cm^{-1} was assigned to C=O vibrations. The asymmetric stretch occurred at 1385 cm^{-1} and symmetric stretch occurred at 1187 cm^{-1} for S=O. In the mass spectrum the peak due to loss of one sodium ion (m/z: 233.2, M-23) can be seen clearly. From ^{1}H NMR spectrum for the product two hydrogens attached to the benzene ring interacted with each other to produce two doublet peaks ($\delta = 7.87$ and 7.48). The UV spectrum of the product ($c = 1 \times 10^{-5}$ in water), which absorbed in 212 (high), 253 (low), and 297 (low) nm, is typical of the manner of benzoic acid derivative. All these data established the formation for the target compound. It was further confirmed by single crystal X-ray diffraction and thermogravimetric analysis.

Crystal structure description

A colorless block crystal of **SPA** with approximate dimensions of 0.20 mm × 0.20 mm × 0.18 mm was selected and mounted on a glass fiber. And the X-ray crystallographic study was carried out using Bruker SMART CCD diffractometer with graphite monochromated Mo-K_α radiation ($\lambda = 0.71073$ Å) at $T = 296(2)$ K. The structure was solved by the direct method and refined by full-matrix least squares procedure against F^2 using the SHELXS-97 and SHELXL-97 programs [17]. The crystal data and structure refinement details for **SPA** are given in Table 1. Selected bond lengths (Å) and angles (°) are listed in Table 2. Crystallographic data have been deposited with the Cambridge Crystallographic Data Centre as supplementary publication, CCDC No. 1037334 for **SPA**. These data can be obtained free of charge via www.ccdc.cam.ac.uk.

Coupled with IR, MS and NMR, X-ray diffraction analysis intuitively provided the crystal structure of **SPA** to us. The crystal lattice of **SPA** belongs to the monoclinic system with a space group *C2/c*. As showed in Fig. 2(a), the crystal **SPA** contains a centrosymmetric dinuclear unit with an inversion center at the center of planar arrangement of Na2, Na2A, O5, and O5A. The asymmetric unit contains two **SPA** molecules, four free water molecules (O4 and O6), and two coordinated water molecules (O5). Figure 2(b) revealed the metal sodium was six-coordinated. Two sodium atoms link two neighboring O5 atoms to form rhombus I. The Na2-Na2 distance in rhombus I is 3.712(3) Å. Two sodium atoms link two neighboring O7 atoms to form another rhombus II connecting to the rhombus I. The Na2-Na2 distance in rhombus II is 9.2352(45) Å. Along the *c*-axis, two sodium atoms are combined with two O1 atoms. Thus, the **SPA** molecules form a 3 D porous network as illustrated in Fig. 2(c). The Na2 atom can be regarded as 6-connected nodes while oxygen atoms act as 2-connected linkers.

The two free water molecules (O4 and O6) acting as the hydrogen bond donor or acceptor. The inter-stack hydrogen bonds are from phenols (O9 and O10) to water (O6) and the sulfonic group (O3). Hydrogen bond distances and bond angles of **SPA** are listed in Table 3.

This is the first published crystal structure study of **SPA**. The structure contains extensive hydrogen bonding within the **SPA** molecule displaying an unusual hydrogen bonding motif.

Table 1. Crystallographic data for **SPA**.

Compound	SPA
Formula	$C_7H_{11}NaO_{10}S$
Color/shape	Colorless/block
Formula weight	310.21
Temperature	296(2) K
Wavelength (Å)	0.71073
Crystal system, space group	Monoclinic, C2/c
Unit cell dimensions	
a (Å)	24.756(12)
b (Å)	6.558(3)
c (Å)	17.589(8)
α (°)	90.00
β (°)	124.508(4)
γ (°)	90.00
Volume (Å^3)	2353(2)
Z	8
$D_{calc.}$ (Mg m^{-3})	1.751
Absorption coefficient (mm^{-1})	0.361
F(000)	1280
Crystal size	0.20 × 0.20 × 0.18
θ range for data collection (°)	$2.00 < \theta < 25.00$
hkl limit	$-15 \le h \le 29$; $-7 \le k \le 7$; $-20 \le l \le 20$
Reflections collected	5986
Unique reflections	2062 [R(int) = 0.0206]
Completeness to $\theta = 25.000$	99.5%
Data/restraints/parameters	2062/0/173
Goodness-of-fit on F^2	1.070
R indices [$I > 2\sigma(I)$]	$R_1 = 0.0614$, $wR_2 = 0.1541$
R indices (all data)	$R_1 = 0.0629$, $wR_2 = 0.1562$
Largest diff. features (e Å^{-3})	0.647 and –1.343

The structure was solved by direct methods and refined by full-matrix least-squares fitting on F^2 by SHELXL-97.

This information may help to explain further the occurrence and role of sodium 5-carboxy-2,3-dihydroxybenzenesulfonate as a potential antioxidant.

Thermal analysis

The thermogravimetric analysis for **SPA** was carried out from 25 to 800°C. Figure 3 presented the thermogravimetric plot (TG) and derivative thermogravimetry (DTG) plots of **SPA**, where five weight loss steps existed. Good agreement between experimental and calculated values was observed (Table 4). The first weight loss stage may be related to the removal of two free water molecules ($T_{max} = 87.69$°C), and the second corresponds to the release of one coordinated water molecule ($T_{max} = 331.82$°C). When the temperature holds on rising, the anhydrous compound **SPA** decompose gradually, losing one sulfonic group, one carboxyl group and two hydroxyl groups successively.

Biological activities assay. Antioxidant assay of SPA

For antioxidant activities, both DPPH radical scavenging assay and reducing power were employed. The DPPH radical scavenging activities of **PA**, **SPA**, and ascorbic acid are shown in Fig. 4(a). It was demonstrated that the DPPH radical scavenging activities of three samples increased concentration-dependent manner. Radical scavenging activities of **SPA** (IC_{50}, 30 μM) and ascorbic acid (25 μM) were higher than that of **PA** (52 μM) for the DPPH radical.

Table 2. The bond lengths (Å) and angles (°) for **SPA**.

Bond dist.	Bond dist.
Na2-O9 2.368(2)	C1-O7 1.221(3)
Na2-O5 2.399(2)	C1-O8 1.319(4)
Na2-O1#1 2.445(3)	C1-C2 1.487(3)
Na2-O7#2 2.461(2)	C2-C3 1.382(4)
Na2-O5#3 2.465(3)	C2-C7 1.397(4)
Na2-O10 2.468(2)	C3-C4 1.394(4)
Na2-Na2#3 3.712(3)	C4-C5 1.403(4)
S1-O1 1.449(2)	C5-O10 1.352(3)
S1-O2 1.450(2)	C5-C6 1.404(4)
S1-O3 1.461(2)	C6-O9 1.363(3)
S1-C4 1.771(3)	C6-C7 1.376(4)
O1-Na2#4 2.445(3)	O7-Na2#2 2.461(2)
O5-Na2#3 2.465(3)	
Angle (°)	Angle (°)
O9-Na2-O5 175.89(8)	O2-S1-C4 107.29(12)
O9-Na2-O1#1 81.44(8)	O3-S1-C4 105.90(13)
O5-Na2-O1#1 94.50(8)	O7-C1-O8 122.8(2)
O9-Na2-O7#2 85.48(8)	O7-C1-C2 124.3(2)
O5-Na2-O7#2 95.61(9)	O8-C1-C2 112.8(2)
O1#1-Na2-O7#2 95.65(8)	C3-C2-C7 119.9(2)
O9-Na2-O5#3 98.63(9)	C3-C2-C1 120.5(2)
O5-Na2-O5#3 80.53(9)	C7-C2-C1 119.6(2)
O1#1-Na2-O5#3 88.49(8)	C2-C3-C4 119.8(2)
O7#2-Na2-O5#3 174.57(9)	C3-C4-C5 120.9(2)
O9-Na2-O10 64.50(7)	C3-C4-S1 118.03(19)
O5-Na2-O10 119.50(8)	C5-C4-S1 121.06(19)
O1#1-Na2-O10 145.77(9)	O10-C5-C4 126.1(2)
O7#2-Na2-O10 85.45(8)	O10-C5-C6 115.7(2)
O5#3-Na2-O10 93.10(8)	C4-C5-C6 118.2(2)
O9-Na2-Na2#3 138.10(8)	O9-C6-C7 123.5(2)
O5-Na2-Na2#3 40.93(6)	O9-C6-C5 115.7(2)
O1#1-Na2-Na2#3 91.91(7)	C7-C6-C5 120.8(2)
O7#2-Na2-Na2#3 136.42(7)	C6-C7-C2 120.4(2)
O5#3-Na2-Na2#3 39.60(5)	S1-O1-Na2#4 126.50(12)
O10-Na2-Na2#3 110.75(7)	Na2-O5-Na2#3 99.47(9)
O1-S1-O2 111.90(14)	C1-O7-Na2#2 124.36(18)
O1-S1-O3 111.66(14)	C6-O9-Na2 119.87(15)
O2-S1-O3 112.39(15)	C5-O10-Na2 117.21(14)
O1-S1-C4 107.28(12)	

Symmetry transformations used to generate equivalent atoms: #1: x, -y + 1, z + 1/2; #2: -x+1/2, -y+3/2, -z+1; #3: -x, -y+1, -z+1; #4: x, -y+1, z-1/2.

Table 3. Hydrogen bond distances (Å) and bond angles (°) in **SPA**.

D–H···A	d(D–H)	d(H···A)	d(D···A)	<DHA
O4-H4C··· O2#5	0.850	1.979	2.817	168.51
O4-H4D··· O3	0.850	2.084	2.922	168.59
O4-H4D··· S1	0.850	2.864	3.673	159.77
O5-H5A··· O4#6	0.850	2.092	2.909	161.17
O5-H5B··· O2#7	0.850	2.347	2.998	133.71
O6-H6A··· O2#8	0.850	2.098	2.941	171.55
O6-H6B··· O1#9	0.850	2.048	2.890	171.07
O8-H8··· O4#10	0.820	1.824	2.641	174.50
O9-H9C··· O6	0.850	1.796	2.646	179.79
O10-H10C··· O3	0.850	1.965	2.644	136.06
O10-H10C··· O3#11	0.850	2.258	2.888	130.91

Symmetry transformations used to generate the equivalent atoms: #5: x, y-1, z; #6: x, -y+1, z+1/2; #7: -x, y, -z+1/2; #8: -x+1/2, -y+3/2, -z+1; #9: -x+1/2, -y+1/2, -z+1; #10: x+1/2, -y+1/2, z+1/2; #11: -x, y, -z+1/2.

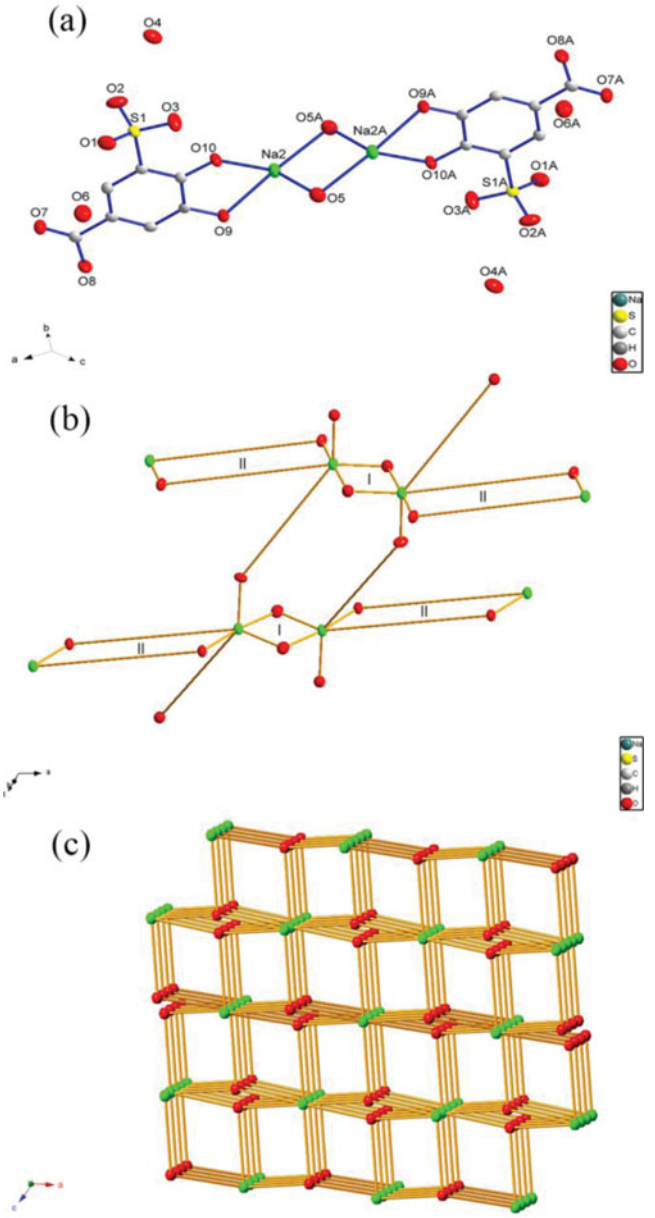

Figure 2. (a) Molecular structure of **SPA** with 50% thermal ellipsoids. (b) The schematic of rhombus I and II framework in **SPA**. (c) Schematic view of the 3 D porous network in **SPA**. All the hydrogen atoms are omitted for clarity.

Figure 4(a) demonstrated that, at the low concentration examined ($<15\ \mu$M) three samples displayed statistically similar inhibition capability on DPPH radical scavenging. At the higher concentration ($>20\ \mu$M) **SPA** exhibited a little stronger DPPH scavenging activity than that of **PA**. Compared with ascorbic acid, **SPA** and **PA** both exhibited moderate DPPH scavenging activity. Figure 4(b) revealed the kinetic behavior of different concentrations of **SPA** on DPPH scavenging activity. Radical scavenging activity of **SPA** was increased in not only a dose- but a time-dependent manner. The DPPH scavenging activity of the raw material **PA** in essence was due to hydrogen atom or single electron transfer from the two vicinal hydroxyl groups at

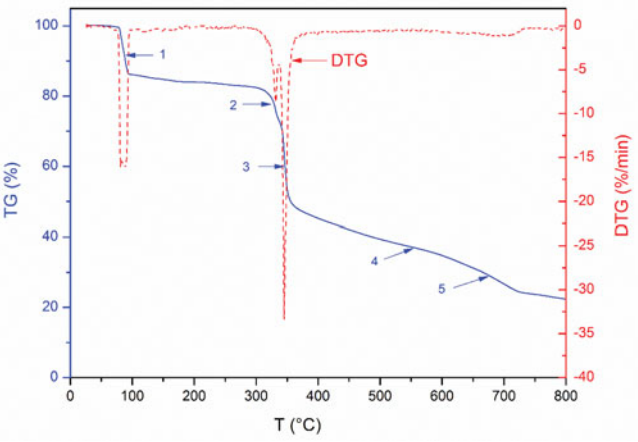

Figure 3. The TG-DTG curves of **SPA**.

Table 4. The maximum speed of the process (T_{max}) and the mass decrement during the heating process of SPA determined from TG and DTG curves

Stage	The loss content	T_{max} (°C)	ΔW (%)	Calcd. (%)
1	two free water molecules	87.69	12.79	11.62
2	one coordinated water molecule	331.82	6.40	5.81
3	one sulfonic group	345.02	25.96	25.81
4	one carboxyl group	—	13.88	14.51
5	two hydroxyl groups	—	10.81	10.96

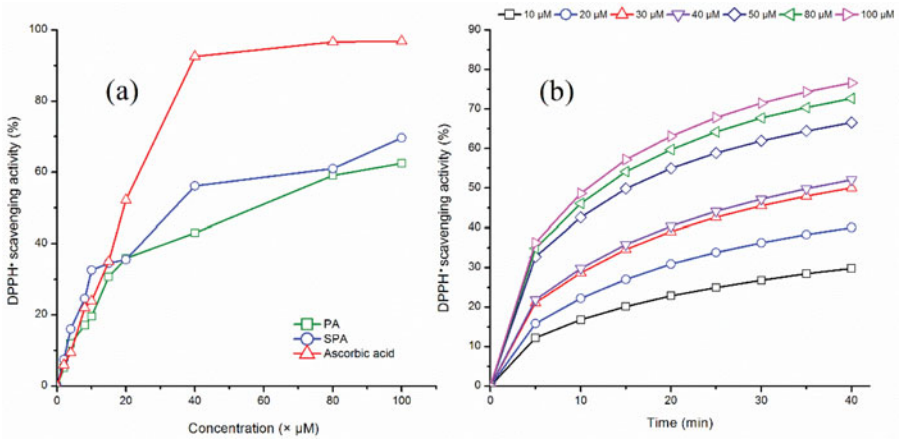

Figure 4. (a) DPPH scavenging activities of **PA**, **SPA** and ascorbic acid; (b) kinetic behavior of DPPH radical scavenging activities of **SPA**.

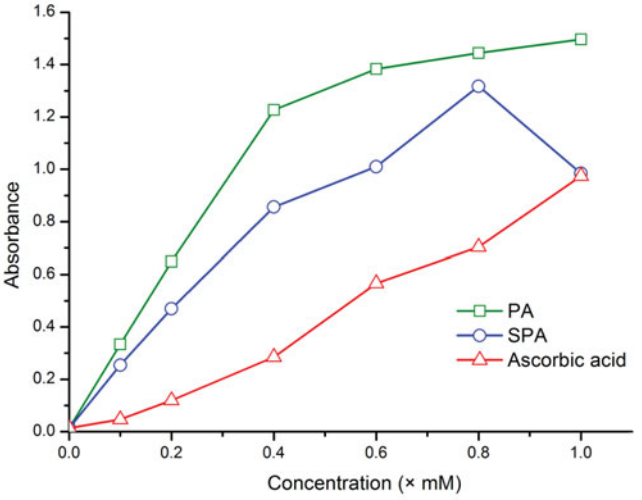

Figure 5. Reducing power (absorbance) of different concentrations of **PA**, **SPA**, and ascorbic acid.

the benzene ring [18]. The better antioxidant activity for **SPA** may be attributed to significant contribution of the sulfonic group in its structure for DPPH radical.

As shown in Fig. 5, the reducing power of **PA**, **SPA**, and ascorbic acid increased with concentration. **PA** and **SPA** displayed more effective reducing power when compared to the positive control, ascorbic acid. It might be partly due to the presence of the two vicinal hydroxyl groups at the benzene ring. However, the derivative **SPA** has been found to show a weaker reducing power than the raw material **PA**. The reason may be explained by the vital influence of the sulfonic group which was introduced by sulfonation.

Isothermal titration calorimetry of the binding of SPA to HSA

The isothermal titration calorimetric profile was obtained from the titration of 1000 μM **SPA** with 50 μM HSA at 25°C. As shown in Fig. 6(a), the ITC titrations yielded negative heat deflection, which indicated that the binding was an exothermic process with a high affinity constant ($K_b = 2.58 \times 10^5$ L/mol). From Fig. 6(b), the fitting curve (solid line) shows well agreement with experimental data represented by the square symbols. Total enthalpy change, total entropy change and total Gibbs free energy change ($\Delta H = -4.005$ kJ/mol, $\Delta S =$ 90.0 J/mol/K, and $\Delta G = -30.84$ kJ/mol) suggested that binding is entropically favored. The slight negative value of the enthalpy and the positive value of entropy in this binding suggests that the interaction is mostly electrostatic in nature [19]. **SPA**, in a sodium salt form, is a negatively charged ion in phosphate buffer solution and is expected to bind at the site consisting of positively charged amino acid residues in the binding cavity of the HSA protein.

Circular dichroism studies

Far-UV circular dichroism spectra of HSA in the absence and presence of different molar concentration ratios of **SPA** were studied to obtain the information on the secondary structures of HSA. From Fig. 7, two negative absorption bands with minima were observed at 208 nm and 220 nm, which were typical of the α-helical structure of HSA [20]. The CD data were expressed in terms of mean residual ellipticity (*MRE*, deg cm^2 dmol^{-1}) calculated from the

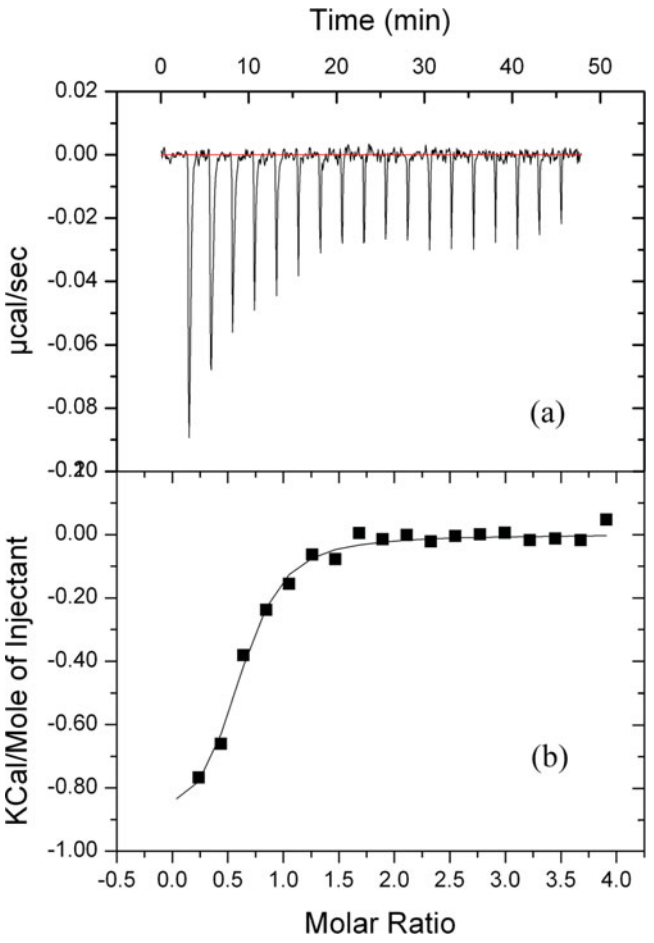

Figure 6. (a) Raw data for the titration of 1000 μM **SPA** with 50 μM HSA at 25°C, showing the calorimetric response as successive injections of the ligand are added to the sample cell. (b) Integrated heat profile of the calorimetric titration shown in panel (a). The solid line represents the best nonlinear least-squares fit to a single binding-site model.

observed ellipticity in degrees as [21]:

$$MRE = \frac{\text{Observed CD}(medg)}{C_p nl \times 10} \tag{2}$$

where is the CD in milli degree, C_p is the concentration of the protein (1.0×10^{-5} mol/L), n is the number of amino acid residues (in HSA $n = 585$), and 0.1 is the path length of the cell (cm).

The α-helical contents of free and combined HSA were calculated from the *MRE* value at 208 nm using Eq. (3):

$$\alpha - \text{Helical}(\%) = \frac{-MRE_{208} - 4000}{33000 - 4000} \times 100 \tag{3}$$

where MRE_{208} is the observed *MRE* value at 208 nm, 4000 is the *MRE* of the β-form and random coil conformation cross at 208 nm, and 33000 is the *MRE* value of a pure α-helix at 208 nm.

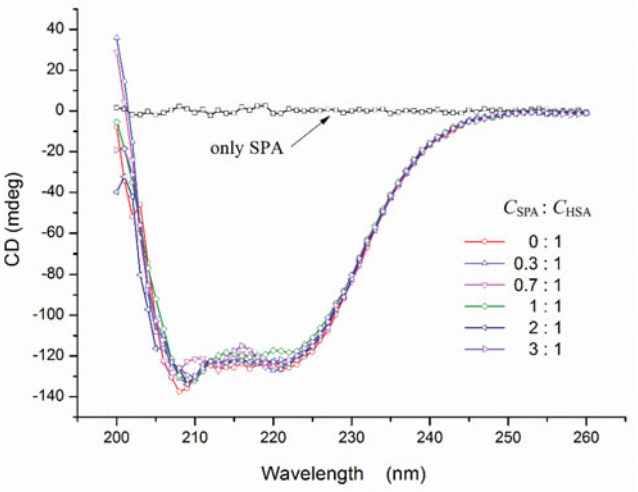

Figure 7. Circular dichroism spectra of HSA in the absence and presence of increasing amount of **SPA** at different molar concentration ratios. $C_{\mathbf{SPA}}$: C_{HSA} for 0:1, 0.3:1, 0.7:1, 1:1, 2:1, and 3:1, respectively; $C_{HSA} = 1.0 \times 10^{-5}$ mol/L, and T = 25°C.

Table 5. The secondary structure determination for free HSA and its coordination compounds for **SPA** and HSA

$c_{\mathbf{SPA}}$: c_{HSA}	0 : 1	0.3 : 1	0.7 : 1	1 : 1	2 : 1	3 : 1
α-Helix (%)	67.72	63.43	61.37	62.56	60.06	60.37

From the above equation, the α-helical contents of free HSA and its drug complexes were determined and shown in Table 5. In the presence of increasing molar concentration ratio of **SPA** with HSA, no appreciable conformational changes in the secondary structure of the protein is observed. The results show that upon binding to the protein **SPA** do not cause any significant denaturation in the secondary structure of HSA, even if the binding constant is strong inferred from the ITC experiment.

Conclusions

In this work, we report the synthesis and characterization of a sulfonated derivative of protocatechuic acid. The compound, sodium 5-carboxy-2,3-dihydroxybenzenesulfonate (**SPA**), was characterized by IR, MS, NMR spectrum, X-ray diffraction analysis and thermal analysis. DPPH scavenging assay and reducing power assay were operated to evaluate the antioxidant effects of **SPA**. At the higher concentration **SPA** exhibited a little stronger DPPH scavenging activity than that of the raw material **PA**. In the kinetic behavior of DPPH scavenging assays, **SPA** revealed a dose- and time-dependent manner on radical scavenging activity. In reducing power assays **SPA** also presented dose-dependency. Compared with the ascorbic acid **PA** and **SPA** displayed more effective reducing power. The sulfonic group close to the two vicinal hydroxyl groups at the benzene ring brought about better DPPH radical scavenging activity but weaker reducing power of **SPA**. The values of binding enthalpy (ΔH), binding entropy (ΔS) and binding constant (K_b), have been measured using isothermal titration calorimetry. The binding constant (K_b) of the order of 10^5 suggested the binding of **SPA** with HSA was

strong. Thermodynamic study indicated that binding interaction was spontaneous in nature and electrostatic interactions were the dominant binding forces. Circular dichroism studies revealed the addition of **SPA** into HSA does not bring about any appreciable perturbation of the secondary structure in HSA. Overall, as the sulfonated derivative of protocatechuic acid, **SPA** exist excellent thermostability and antioxidant effects. The strong binding interactions of **SPA** with HSA would have important implications in the drug design. Further studies on the analogues of **SPA** are needed in the future, for developing phenolic compounds with desired antioxidant and physiological potential.

Acknowledgments

This work was financially supported by the Natural Science Foundation of China (21362001), and Natural Science Foundation of Guangxi Province (2013GXNSFDA019005).

References

[1] Harborne, J. B. (1980). In: *Encyclopedia of Plant Physiology*, Charlwood: Bell, AE, 8, 329.
[2] Stalikas, C. D. (2007). *J. Sep. Sci.*, *30*, 3268.
[3] (a)Huang, L. et al. (2010). *Nat. Prod. Commun.*, *5*, 1263; (b)Cai, Y. Z.,Luo, Q.,Sun, M., & Corke, H. (2004). *Life Sci.*, *74*, 2157; (c)Ghasemzadeh, A., & Ghasemzadeh, N. (2011). *J. Med. Plants Res.*, *5*, 6697; (d)Hadi, S. M., Asad, S. F.,Singh, S., & Ahmad, A. (2000). *IUBMB Life*, *50*, 167.
[4] Shahidi, F., Wanasundara, P. D., & Janitha, P. K. (1992). *Crit. Rev. Food Sci. Nutr.*, *32*, 67.
[5] (a)Sroka, Z., & Cisowski, W. (2003). *Food Chem. Toxicol.*, *41*, 753; (b)Rice Evans, C.,Miller, N. J., & Paganga, G. (1996). *Free Radical Biol. Med.*, *20*, 933.
[6] (a)Jalaja Kumari, D. (2012). *Int. J. Pharm. Res. Bio-Sci.*, *1*, 166; (b)Zhao, L. G. et al. (2014). *J. Asian Nat. Prod. Res.*, 16, 677; (c)Halder, S. K. et al. (2014). *Food Chem.*, *158*, 325; (d)Liu, Q. et al. (2014). *J. Agric. Food Chem.*, *62*, 8858.
[7] (a)He, X. M., & Carter, D. C. (1992). *Nature (London)*, *358*, 209; (b)Khodarahmi, R. et al. (2012). *Spectrochim. Acta, Part A*, *89*, 177.
[8] (a)Meng, F. Y., Zhu, J. M., Zhao, A. R., Yu, S. R., & Lin, C. W. (2012). *J. Lumin.*, *132*, 1290; (b)Luo, X. et al. (2013). *Luminescence*, *28*, 202; (c)Wei, J. et al. (2014). *Proc. Natl. Acad. Sci., India, Sect. A*, *84*, 505.
[9] Bouchemal, K. (2008). *Drug Discov. Today*, *13*, 960.
[10] Falconer, R. J., & Collins, B. M. (2011). *J. Mol. Recognit.*, *24*, 1.
[11] Frost, J. W., & Bui, V. (2011). Sulfonation of polyhydroxyaromatics. Patent WO2011022588A1.
[12] Blois, M. S. (1958). *Nature (London, UK)*, *181*, 1199.
[13] Oyaizu, M. (1986). *Japanese J. Nutr.*, *44*, 307.
[14] Hayat, K. et al. (2010). *Food Chem.*, *123*, 423.
[15] Jiang, B. et al. (2013). *J. Chem. Pharm. Res.*, *5*, 1529.
[16] Liu, M. et al. (2007). *J. Chem. Thermodyn.*, *39*, 1565.
[17] Sheldrick, G. M. (2008). *Acta Crystallogr., Sect. A: Found. Crystallogr.*, *64*, 112.
[18] (a)Zhou, X. J. et al. (2010). *J. Asian Nat. Prod. Res.*, *12*, 399; (b)Wang, M. F., Jin, Y., & Ho, C. T. (1999). *J. Agric. Food Chem.*, *47*, 3974.
[19] Ross, P. D., & Subramanian, S. (1981). *Biochemistry*, *20*, 3096.
[20] Kandagal, P. B. et al. (2006). *J. Pharm. Biomed. Anal.*, *41*, 393.
[21] Tabassum, S., Al-Asbahy, W. M., Afzal, M., & Arjmand, F. (2012). *J. Photochem. Photobiol., B.*, *114*, 132.